CrossMark

A Zonal Different-Time-Step Algorithm for Multi-Physics Simulation in Closed System

Ke Wu[1] · Kai Zhu[1,2] · Xin Zhang[1] · Cheng Kang[1] · Yanji Wei[1,3]

Abstract In the present paper, a Zonal Different-Time-Step algorithm (ZDTS) is developed to overcome the difficulties of the flow, chemical reaction and heat transfer couple simulation in a domain-closed system. The system is decomposed into reaction zone and flow zone. The CFD simulations are performed in each zone individually, using different characteristic times, the physical information is effectively passed via interpretation at the interface. A case study of shell-and-tube reactor is presented for the validation. Numerical simulation based on ZDTS is performed to understand the catalytic reaction in porous media at tube side and the flow and heat transfer of the molten salt at shell side. The effects of selected interpolation methods and asynchronous factor (Af) on the computational accuracy and efficiency are investigated. The numerical results show that the ZDTS provides the details of flow field and heat transfer at different zones, predicts the accurate positions of the stagnation zones and the dead zones accurately, and reveals the characteristic of the heat transfer between each zone. The ZDTS significantly increases the computation efficiency by 50 %, and the numerical results show good agreement with the measured results. The ZDTS can be applied for the flow, chemical reaction and heat transfer couple simulation in a closed domain.

Keywords Zonal different-time-step algorithm · Multi-physics system · Chemical reaction · Heat transfer · CFD

✉ Yanji Wei
  yanji.wei@ucdconnect.ie

  Ke Wu
  wuke@zju.edu.cn

  Kai Zhu
  zhukaizju@zju.edu.cn

  Xin Zhang
  siyecao1013@126.com

  Cheng Kang
  gronckle_kang@163.com

1 Faculty of Engineering, Zhejiang University, Hangzhou 310027, China

2 College of Quality and Safety Engineering, China Jiliang University, Hangzhou 310018, China

3 School of Mathematics and Statistics, University College Dublin, Belfield, Dublin4, Ireland

1 Introduction

Multi-physics system involving flow, chemical reaction and heat transfer is common in nature, which is multi-factor-dependent system. The common CFD model for heat transfer simulation generally takes into account only one of the factors [4]. Shell-and-tube reactor is such a typical Multi-physics system. It is a shell container with thousands of tubes inside which separates the domain into two zones. When computing the flow and heat transfer at shell side, the heat releasing rate of the reaction at tube side is considered as a fixed boundary condition; when computing the chemical reaction at tube side, a formulated heat transfer coefficient at shell side is used for the computation [14, 15]. However, such simplifications ignore the heat exchange between the shell side and the tube side. The great variation of the flow at shell side may significantly change the heat transfer rate at tube side, which may affect the temperature distribution and the reacting rate at tube side, and the temperature at shell side may be altered consequently.

Therefore, ignoring the multi-physical coupling effects may introduce unexpected errors into the numerical model. The CFD simulation at two sides can be performed in one integrated model to take into account the interaction between them. The difficulty is that the time scales of the variables at two sides are significantly different, the time step in CFD model has to be compatible with the smallest time scales, which makes the model inefficient. Development of numerical algorithm with higher computational efficiency while keeping the accuracy of the model is of great value.

Two strategies are commonly used to deal with the multi-physics problems: one is the integral method that considers the closed system as one domain which is governed by uniform equations, thus the shell side and the tube side are solved simultaneously; another is the zonal method which decomposes the domain into several individual sub-zones, each sub-zone is governed by different conservation equations and solved independently, while the data swaps at the interfaces to take into account the interaction between them. The chemical reaction zone and the heat transfer zone are relatively independent in the system for some cases [3, 7, 10]. They don't exchange mass but energy between two zones, i.e. typical closed systems. The zonal method is an ideal method for these classes of multi-physical problems. With zonal method, numerical model may contain several individual modules. Each module is developed to deal with the physical field in one sub-zone using state-of-the-art solutions. This method has been successfully employed in a wide range of engineering problems, e.g. chemical reactor network for combustion [11], aero-thermal coupling analysis for hypersonic vehicles [18] and coupled flow-thermal-structural analysis [19]. However, by using the traditional zonal method, solving the chemical reaction, turbulent flow and heat transfer in each sub-zone simultaneously is not an easy job sometimes, which computational cost may be expensive and require high-performance computational facility. Hence, the development of the cost-effective zonal algorithm has attracted many researchers [16, 17].

In the present paper, we firstly purpose a zonal different-time-step algorithm aiming to simulate the flow, chemical reaction and heat transfer couple system in a closed domain in Section 2. Afterwards, we present a case study of shell-and-tube reactor in order to validate the purposed method in Section 3. Finally, we analyse the flow and heat transfer in the reactor using the numerical results in Section 4.

2 Zonal Different-Time-Step Algorithm

In flow, chemical reaction and heat transfer couple problems, the energy distribution in a closed system is dominated by both the heat released in chemical reaction and the convective heat transfer. The hydrodynamic conditions and the governing equations are different in the flow zone and the reaction zone, hence the solving algorithm may vary in different zones. Taking the widely used shell-and-tube reactor [12] as an example, its reaction zone (tube side) contains hundreds (or even thousands) of reaction tubes. The flow in these tubes can be described as a sum of Poiseuille flow and Knudsen flow with weak non-linearity, which may converge quickly in the simulation. On the other hand, the heat transfer in flow zone (shell side) is a forced convection heat transfer with large Reynolds number, in which the flow are highly non-linear hereby the computation is costly. Furthermore, the reaction tubes are generally filled with high porosity catalyst, the characteristic time of the heat transfer in the porous tubes is of the order of seconds, while the characteristic time of the turbulent flow at shell side is of the order of milliseconds. In order to ensure the precision of the flow prediction and improve the accuracy of the iteration, a smaller time step is preferable in flow zone. The computational cost may significantly increase if applying the same time step in reaction zone as that adopted in flow zone, although that would not be very conducive to more accurate results. Based on the principal of heat transfer, the temperature variation on the wall in a short time is small and such influence on the flow is limited in the boundary layer only, even if there is large heat flux on the wall. Hence, the flow in flow zone can be considered as steady flow in a short time, i.e. the characteristic time of the reaction zone. Smaller time step is applied in the flow zone to obtain higher accuracy, whereas larger time step is applied in the reaction zone to reduce computational cost.

According to the upon discussion, the flowchart of the ZDTS is shown in Fig. 1. The ZDTS assumes that the reaction zone and the flow zone are physically decomposed in domain. There is only heat exchange rather than mass exchange between two zones in a shell-and-tube reactor. The flow zone and the reactor zone are solved individually using different time steps, and pass the physical information between them at the interface. This method can be implemented by following the steps:

1. Carry out the steady simulation in reaction zone at t_0 and calculate the wall heat flux density q at the interface;
2. Perform the unsteady simulation with time step of t_f in flow zone, using the heat flux density q obtained in the previous step as the boundary condition;
3. Transfer the convection heat transfer coefficient h_f in flow zone into h_r in reaction zone by interpolation;
4. Restart the simulation in reaction zone from t_0 to $t_0 + t_r$ with h_r as input at wall boundaries, export the wall heat flux density q at the end of the simulation for the next iteration;
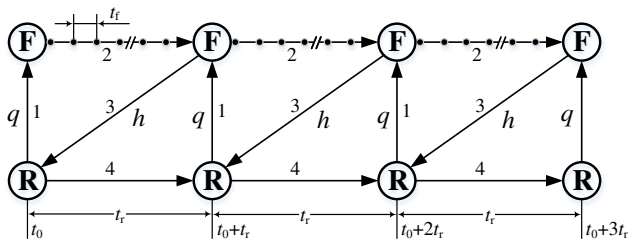
Figure 1 Flowchart of zonal different-time-step algorithm, R represents the reaction zone and F represents the flow zone.

This method can reduce the data exchanging frequency and the computational amount in the reaction zone, therefore greatly speed up the simulation.

The selections of the time steps t_f and t_r are critical in the ZDTS algorithm. Theoretically, t_f and t_r should be the same order as the characteristic times of the flow zone and the reactor zone respectively. However, due to the complex boundary conditions and the complicated structures of the reactor, the system involves various flow patterns. The characteristic time may vary locally, depending on the flow conditions. In order to properly estimate t_f and t_r, we introduce a asynchronous factor Af ($Af = t_r/t_f$) in the model to balance the accuracy and the efficiency.

Because the governing equations in flow zone and reaction zone are different, the meshing schemes in each zone may be different. The mesh is generated independently in each zone and the patched grid scheme [5] is used to bridge the zones by the interface. Patched grid dose not need conformal mesh at the interface, hence it can simply the mesh generation process. More important, thanks to the non-conformal interface, the mesh in each zone can be optimised independently, which may reduce the mesh number thus the computational cost.

The interpolation method has to be used in order to pass the physical data between the non-conformal interfaces. The selection of the interpolation methods may influence the accuracy of the numerical results, which is investigated in Section 4.1

3 CFD Model Description

In the present paper, we use the shell-and-tube reactor for catalytic oxidation of HCl as a test case. Because the reaction zone and the flow zone are solved independently, the numerical solutions are described separately, i.e. governing equations, boundary conditions, meshes and numerical schemes. Following the steps of the ZDTS as stated in Section 2, the simulations in two zones are performed alternately to obtain the final results.

3.1 Shell-and-Tube Reactor

The reactor is decomposed into two zones, namely the reaction zone (at tube side) and the flow zone (at shell side). The flow zone is divided into three individual parts by the tube sheets. Each part is 1570 mm in length and 700 mm in internal diameter, as shown in Fig. 2. 142 reaction tubes ($\Phi 32$ in external diameter) and 6 tie rods ($\Phi 16$ in external diameter) are assembled into a ring array in the form of equilateral triangles. The fluid in the flow zone is molten salt, which enters from the bottom of the reactor. The reacting gases flow into reaction tubes from the top. There are 2 baffle plates (560 mm in external diameter) and 3 baffle rings (300 mm in internal diameter) in each part to guide the molten salt flow in flow zone. The flow zone is further divided into 6 sections, which can be classified into four characteristic sections: entrance section (I), exit section (VI), ring-plate sections (II, V) and plate-ring sections (III, V).

3.2 Governing Equations in Reaction Zone

The chemical reaction in the reaction tubes is gas-phase catalytic oxidation of HCl with air or oxygen for producing Cl_2 (see Eq. 1), which is so-called Deacon reaction [1].

$$4HCl + O_2 \rightarrow 2H_2O + 2Cl_2 \tag{1}$$
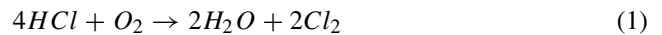
Considering that the reaction tube is filled with catalysts, the flow between the catalyst particles involves Poiseuille flow, Knudsen flow and surface flow [2]. The surface flow
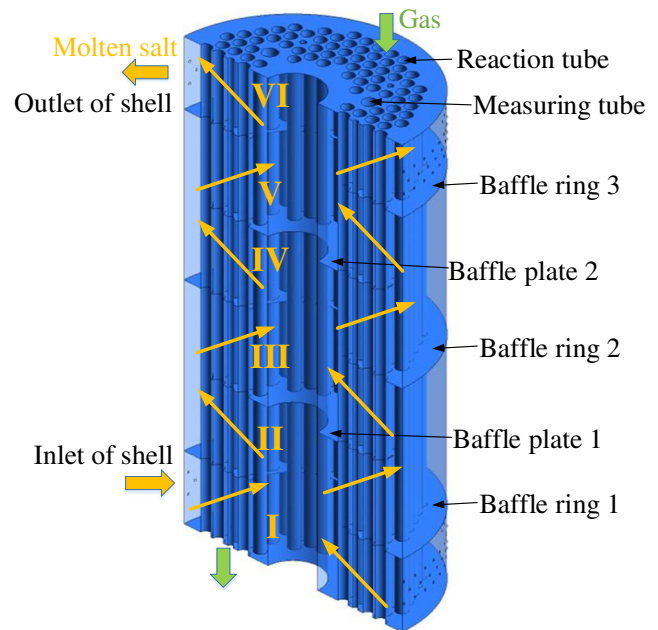

Figure 2 Schematic of an individual part of the reactor, the part is further divided into 6 sections.

is negligible due to the low concentration of the reactant on the surface of the porous media. Hence, the total mass flux $\dot{m}$ is given by:

$$\dot{m} = \rho_g u = \dot{m}_p + \dot{m}_k \tag{2}$$

where $\dot{m}_p$ is the mass flow rate of Poiseuille flow, $\dot{m}_p = -\frac{K}{\mu}\frac{PM}{RT}\nabla P$; $\dot{m}_k$ is the mass flow rate of Knudsen flow, $\dot{m}_k = \frac{\varepsilon_a}{\tau}D_{ek}\frac{M}{RT}\nabla P$; K is a coefficient represents the permeability of the porous media, $K = \frac{\varepsilon_a^3 \times d^2}{150 \times (1-\varepsilon_a)^2}$, according to the semi-empirical Blake-Kozeny equation [6]; D_{ek} is the equivalent diffusion coefficient of Knudsen flow, $D_{ek} = 1/(1/D_m + 1/D_k)$ with $D_m = 0.02628\frac{\sqrt{T^3/M}}{P\sigma^2\Omega}$ and $D_k = \frac{200 r_p}{3}\left(\frac{8RT}{\pi M}\right)^{1/2} = 97 r_p \left(\frac{T}{M}\right)^{1/2}$ [13].

The mass transport of the reacting gas in reaction tubes is governed by:

$$\frac{\partial \rho_{g1}}{\partial t} + \nabla \cdot (\rho_{g1}\mathbf{u}) + \rho_s R_r = 0 \tag{3}$$

where R_r is the reaction rate, which can be estimated by the kinetic parameters of elementary reactions.

The mass transport of the other gases in reaction tubes is described by:

$$\frac{\partial \rho_{g2}}{\partial t} + \nabla \cdot (\rho_{g2}\mathbf{u}) = 0 \tag{4}$$

Defining the apparent permeability coefficient $K_{ap} = K + \frac{\varepsilon_a \mu}{\tau P}D_{ek}$, the gap velocity vector $\mathbf{u}$ can be obtained by Darcy equation:

$$\mathbf{u} = -\frac{K_{ap}}{\mu}\nabla P \tag{5}$$

Substituting the sum of the mass equations Eq. 3 and Eq. 4 and the Darcy equation Eq. 5 into Eq. 2, we obtain the final total mass flow equation:

$$\frac{\partial(\frac{\varepsilon}{RT}P)}{\partial t} = \frac{\partial}{\partial z}\left(\frac{\rho_g K_{ap}}{\mu}\frac{\partial P}{\partial z}\right) + \frac{1}{r}\frac{\partial}{\partial r}\left(\frac{r\rho_g K_{ap}}{\mu}\frac{\partial P}{\partial r}\right) - \rho_s R \tag{6}$$

The energy transport in the porous media in the reaction tubes is calculated by:

$$\begin{aligned}(\rho_s C_{Ps} + \sum \rho_g C_{pg})\frac{\partial T_s}{\partial t} &+ \frac{\partial(\rho_g C_{pg} u T_s)}{\partial z} \\ &+ \frac{1}{r}\frac{\partial}{\partial r}(r\rho_g C_{pg} v T_s) \\ = \frac{\partial}{\partial z}\left(\lambda_{eq}\frac{\partial T_s}{\partial z}\right) &+ \frac{1}{r}\frac{\partial}{\partial r}\left(r\lambda_{eq}\frac{\partial T_s}{\partial r}\right) + \rho_s R\Delta H \end{aligned} \tag{7}$$

where λ_{eq} is the equivalent thermal conductivity. In practice, the values of the thermal conductivity used in numerical models were commonly obtained via experiments. With the experimental input, the numerical models can be used to predict the system performance and optimize the adsorbent configurations. In the present paper, λ_{eq} is calculated

by Eq. 8 proposed by Hsu et al. [9]. Equation 8 has been applied in the isothermal heat transfer model for porous media, and the computed results show good agreement with the experimental results.

$$\lambda_{eq}/\lambda_f = \frac{r_a r_c}{\Lambda} + \frac{r_a(1-r_c)}{1+(\Lambda-1)r_c} + \frac{(1-r_a)}{1+(\Lambda-1)r_a r_c} \tag{8}$$

where λ_g and λ_s are the thermal conductivity of reaction gas and catalyst particle; $\Lambda = \lambda_g/\lambda_s$; r_a and r_c are the model constants.

3.3 Governing Equations in Flow Zone

The molten salt convective and conductive heat transfer at shell side is governed by the continuity equation, momentum equations and energy equation. Assuming that the molten salt flow is incompressible steady flow, which continuity equation is written as:

$$\frac{\partial u_i}{\partial x_i} = 0 \tag{9}$$

and the momentum equations are written as:

$$\frac{\partial \rho u_i u_j}{\partial x_j} = -\frac{\partial p}{\partial x_i} + \frac{\partial}{\partial x_j}\left[\mu\left(\frac{\partial u_i}{\partial x_j} + \frac{\partial u_j}{\partial x_i}\right)\right] + \frac{\partial(-\rho\overline{u_i' u_j'})}{\partial x_j} \tag{10}$$

The $k-\varepsilon$ turbulence model is used to close the Reynolds-stress equations, and the k and ε equations are written as:

$$\begin{aligned}u_j\frac{\partial(\rho k)}{\partial x_j} = \mu_t\left(\frac{\partial u_i}{\partial x_j} + \frac{\partial u_j}{\partial x_i}\right)\frac{\partial u_i}{\partial x_j} - \rho\varepsilon \\ + \frac{\partial}{\partial x_j}\left[(\mu + \frac{\mu_t}{\sigma_k})\frac{\partial k}{\partial x_j}\right]\end{aligned} \tag{11}$$

$$\begin{aligned}u_j\frac{\partial(\rho\varepsilon)}{\partial x_j} = &\frac{\partial}{\partial x_j}\left[(\mu + \frac{\mu_t}{\sigma_\varepsilon})\frac{\partial\varepsilon}{\partial x_j}\right] \\ &+ C_{\varepsilon 1}\mu_t\frac{\varepsilon}{k}\left(\frac{\partial u_i}{\partial x_j} + \frac{\partial u_j}{\partial x_i}\right) \\ &\times \frac{\partial u_i}{\partial x_j} - C_{\varepsilon 2}\rho\frac{\varepsilon^2}{k}\end{aligned} \tag{12}$$

where μ_t is the turbulent viscosity, $\mu_t = C_\mu\rho_f k^2/\varepsilon$; $C_{\varepsilon 1}$, $C_{\varepsilon 2}$, C_μ, θ_k and θ_ε are the model constants, $C_\mu = 0.09$, $\theta_k = 0.24$, $\theta_\varepsilon = 0.15$, $C_{\varepsilon 1} = 1.44$, $C_{\varepsilon 2} = 1.92$.

The energy equation is described as:

$$\frac{\partial(\rho h)}{\partial t} + \frac{\partial}{\partial x_j}(\rho u_i h) = \frac{\partial}{\partial x_j}\left(k_T \partial T/\partial x_j - \tau_{ij}u_j\right) + \rho Q_R + S_h \tag{13}$$

where k_T is the generalized diffusion coefficient; Q_R is the energy sources due to radiation and S_h is the energy sources due to chemical reaction.

3.4 Boundary Conditions

The boundary conditions in reaction zone are defined as follow: $z = 0$ is the gas inlet boundary, where $T_s = T_0$, $P = P_{in} = 1.4 \times 10^5$ Pa and $\rho_{g2} = 23.73$ mol/m^3; $z = L$ is the pressure outlet boundary, where $P = P_{out} = 0.7 \times 10^5$ Pa, $\frac{\partial T_s}{\partial z} = 0$ and $\frac{\partial \rho_{g2}}{\partial z} = 0$; the external walls of the reaction tubes are the Robin boundary condition, which couple with the temperature at shell side.

The boundary conditions in flow zone are defined as follow: the inlet is the Dirichlet boundary with constant mass flow rate of molten salt of 8.054 kg/s (or 16 m^3/h), and the temperature is 360 °C; the outlet is the Neumann boundary, the relative static pressure is 0; the internal walls of the shell are the insulated boundary; the baffle plates and the tie rods are the coupled two-sides walls, no additional thermal boundary conditions are required; the external walls of the reaction tubes is the Robin boundary condition, which couples with the temperature at the tube side.

3.5 Mesh Generation

Due to the symmetry of the problem, simulations are performed for half of the model. The triangular prism mesh with maximum mesh size of 4 mm is used in flow zone. Boundary layer mesh is added to the tube walls in order to accurately capture the high wall-normal velocity/temperature gradients. The thickness of the first layer is 0.5 mm with 4 layers of cell extruded with the growth factor of 1.2. The general mesh of the cross section is shown in Fig. 3. The total number of the mesh cells is 12.8 M. The mesh independent study shows that the results are converged for the present mesh.

A polar mesh is employed in reaction zone. Due to the high temperature gradients caused by the large thermal resistance in the reaction tube, very high-resolution mesh is adopted. The mesh size is 0.5 mm in radial direction and 7 mm in axial direction. The number of the mesh cells for a single tube is 79.2 K, and the total number of the mesh cells is 5.62 M.
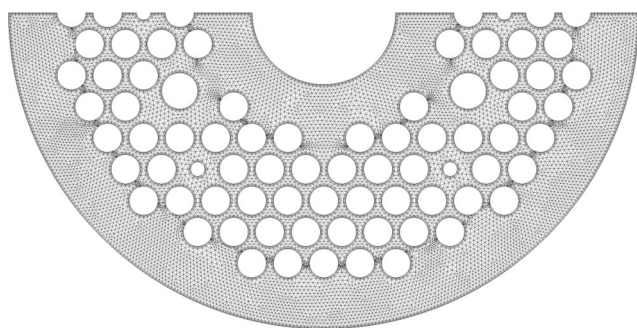
3.6 Numerical Schemes

A finite volume approach is employed in the present simulation. In reaction zone, the convective term, the diffusion term and the unsteady term are discretized by using the power-law scheme, the central difference scheme and the forward difference scheme respectively. The discretized algebraic equations are solved by using a hybrid method which combines a TDMA (Tri Diagonal-Matrix Algorithm) and a Gauss-Seidel method. In flow zone, the central difference scheme is adopted for the diffusion term and the unsteady term while the second order upwind scheme is adopted for the convective term. The Gauss-Seidel method are employed to solve the discretization equations. By implementing the ZDTS stated in Section 2, swapping the physical information between the two zones at every loop, the multi-physics couple system is numerically solved. Convergence of the solution is achieved when the residual is below 1×10^{-3} for velocity and pressure and 1×10^{-6} for energy.

4 Results and Discussion

4.1 Selection of Interpolation Methods

The average temperature of the reaction tube is chosen to investigate the accuracy of the selected interpolation method. Three interpolation methods, i.e. linear interpolation, hybird interpolation and second order interpolation (the details of the interpolation methods can be found in Franklin and Lee [8]), are employed for investigation.

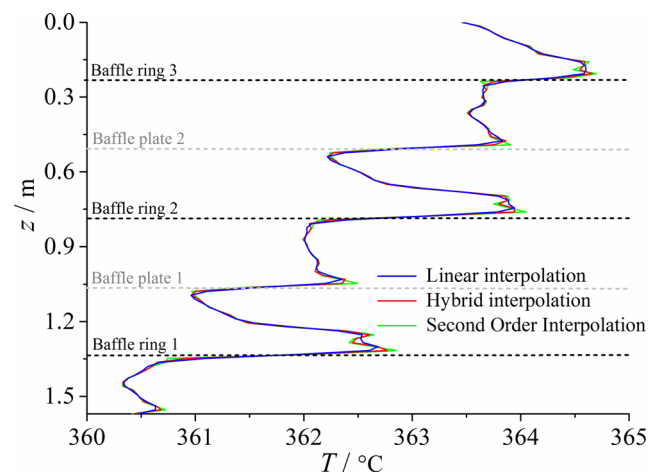The results with three interpolation methods are presented in Fig. 4. They demonstrate good agreement with

Figure 3 Mesh in flow zone.

Figure 4 Variation of average temperature of the reactor tubes with various interpolation methods.

each other, indicating that the general results are not sensitive to the selection of the interpolation methods. However, due to the complex flow in the reactor, the extreme temperature may be observed near the baffle plates/rings, especially for the reactor with complicated structure. As shown in Fig. 4, the higher order method can better describe the sharp variation near the interface between the sections. Hence, it is decided to apply the second order interpolation method in the following studies.

4.2 Asynchronous Factor

Asynchronous factor Af is a parameter representing the data exchanging frequency between the reaction zone and the flow zone. A series of simulations is performed with various value of Af under the same convergence criterion. The iteration numbers and the computational times with $Af = 1, 2, 5, 10, 20, 50$ are shown in Fig. 5. The iteration numbers of the flow zone N_f increase as Af increases, whereas the iteration numbers of the reaction zone N_r decreases at the beginning but keeps constant when $Af \geq 20$. The total computational time slightly declines at the beginning but increases remarkably since $Af \geq 10$, indicating that the optimal Af should be in the range of $5 \sim 10$, which offers the same order of the accuracy while the computational cost is lowest. $Af = 5$ is used in the following studies.

4.3 Characteristics of Exothermic Reaction in Reaction Zone

The temperature in the reaction tubes increases rapidly at the entrance and reaches the maximum at about 1 m away from the entrance, which is contributed by the combined effects of the exothermic reaction at tube side and the heat transfer at shell side. Later, the reaction declines as the decrease of the concentration of the reacting gases. The released heat is exchanged with the molten salt flow at shell side, and the temperature decreases consequently. Because the thermal resistance of the gas-solid heat transfer at the internal wall of the reaction tubes is significantly larger that of liquid-solid heat transfer at the external wall, the core temperature of the tubes is mainly dominated by the chemical reaction. In order to record the time histories of the core temperature in the experiment, thermocouple probes are installed in the centre of the characteristic tubes in the reactor. Figure 6 shows the comparison of the numerical core temperature of the reactor tubes in axial direction with the experimental one. They agrees well with each other, indicating that the ZDTS is an accurate method for the present case.

Because the heat transfer between the gas and the tube walls will be completely absorbed by the molten salt. The experimental heat transfer rate can be estimated by:

$$Q = C_{pf} \rho_f q_f \left(T_{out} - T_{in} \right) \tag{14}$$

where q_f is the flow rate of the molten salt which is measured by the flowmeter and T_{out} and T_{in} are the temperature at the inlet and the outlet of the parts which are measured by the temperature sensors.

The numerical heat transfer rate is compared with the experimental one, as shown in Fig. 7. The results in three parts are in good agreement with each other, the difference is less than ± 10 %.

The numerical results of the heat exchanging rate of the reactor tubes are shown in Fig. 8. The heat exchanging rate at the inlet of the entrance section is negative, then increases rapidly to the positive maximum. That is because there is great temperature difference between the reacting gases and
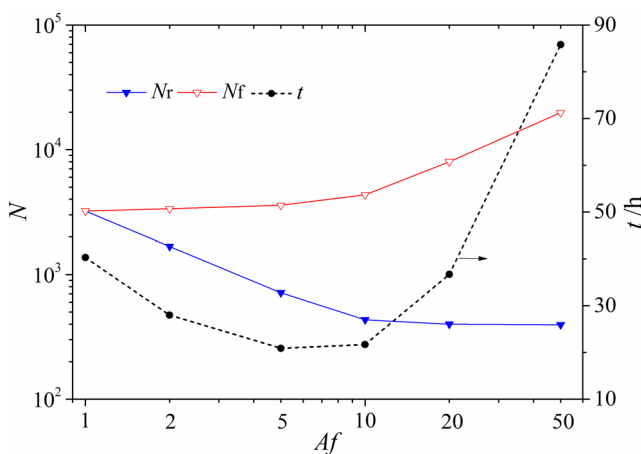
Figure 5 Effects of Af on iteration numbers and computational time. N_r is the iteration numbers of the reaction zone; N_f is the iteration numbers of the flow zone and t is the computational time.
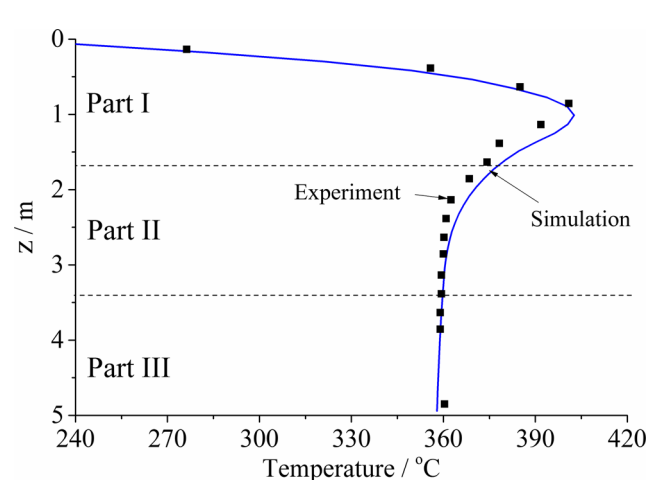
Figure 6 Comparison of core temperature of reactor tubes in axial direction with numerical and experimental results.
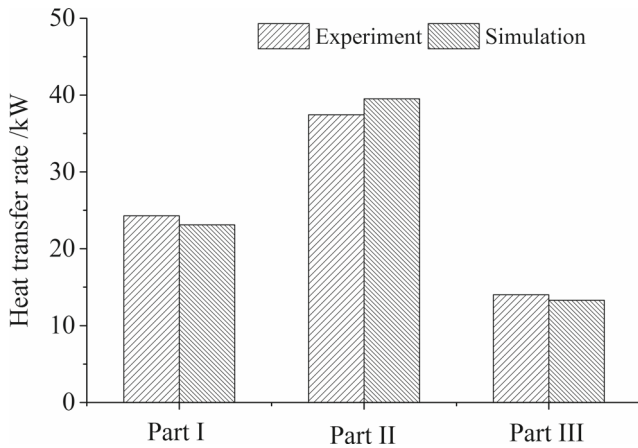
Figure 7 Comparison of heat transfer rate of each part with numerical and experimental results.

Figure 9 Streamlines at shell side, the *red circles* mark the stagnation zones.

the molten salt, the heat transports from the shell side to the tube side, even though the exothermic reaction takes place as soon as the gases entrance the tubes. However, the situation is reversed due to the rapid increasing temperature in the tubes caused by the high reaction rate at the early stage. After that, the concentration of the gases and the reaction rate decreases, resulting in the decrease of the heat releasing rate at tube side. The heat exchanged from the reaction tubes to the molten salt decreases gradually in Parts I and II.

4.4 Characteristics of Flow and Heat Transfer in Flow Zone

The streamlines in the Part II of the reactor at shell side are presented in Fig. 9. The molten salt flow is periodically accelerated or decelerated at shell side due to the alternate presence of the baffle plates/rings, associated with the change of the flow direction, which results in snake-like streamlines as shown in Fig. 9. The stagnation zones and the
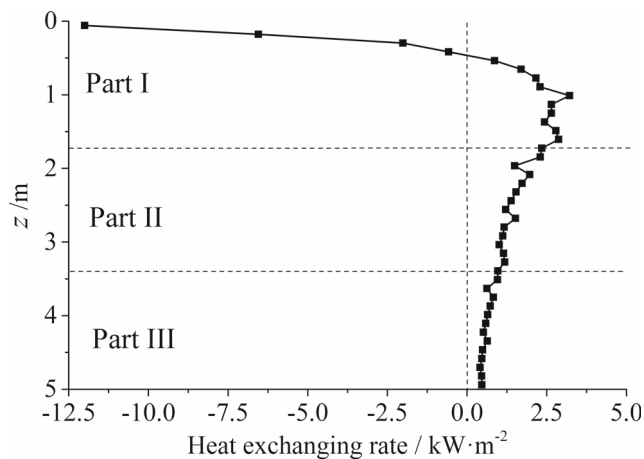

Figure 8 Numerical results of heat exchanging rate of reactor tubes in axial direction.
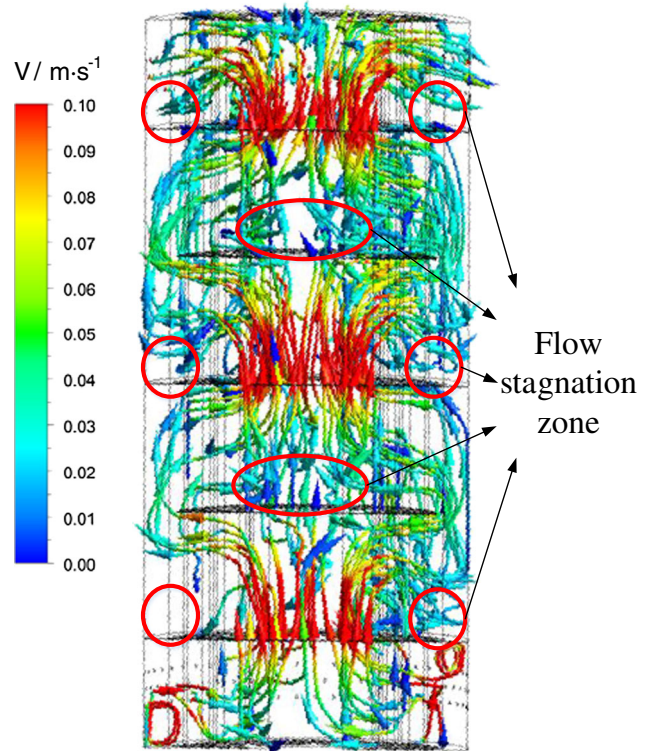
heat transfer dead zones may occur at the back of the baffles where is protected by the baffles. It can be seen in Fig. 9 that the stagnation zones (red circles) are mainly located at the both sides of the baffle rings and the central region of the upper side of the baffle plates.

Three reaction tubes at different positions are selected as examples showing the periodical variation of the temperature on the external walls of the tubes. As shown in Fig. 10, *tube* 1 is close to the shell, *tube* 3 is near the centre of the reactor and *tube* 2 is in between them, the variations of the temperature and the heat exchanging rate are summarized as follow:

1. In the ring-plate sections (II, IV) and the exit section (VI), the flow expands from the centre toward the shell and slows down. The heat exchanging rate decreases from *tube* 1 to *tube* 3 because it is generally proportional to the flow velocity. Hence, the temperature is higher in *tube* 1 than that in *tube* 3.
2. In the plate-ring sections (III, V) and the entrance section (I), the flow sinks into the ring centre, the difference of the heat exchanging rate between three tubes is smaller than the ring-plate sections, implying that the uniformity of the heat exchanging rate in the plate-ring sections is better that in the ring-plate sections.
3. The maximum temperatures on the tubes are commonly observed at the lower regions in each section, where
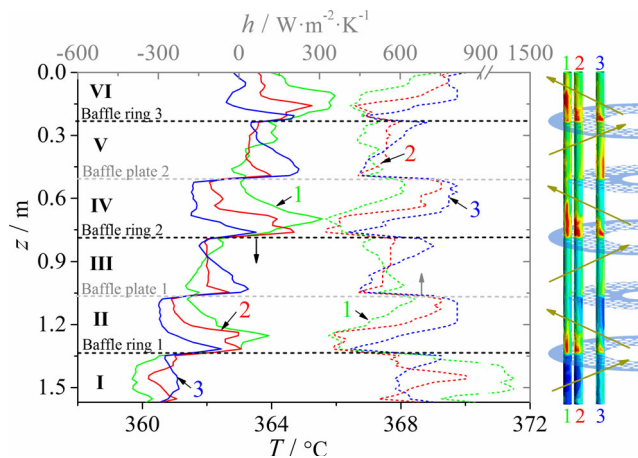
Figure 10 Temperature and heat exchanging rate variations of reactor tubes in axial direction in Part II. The *solid lines* are the temperature variation of the tubes, the *dashed lines* are the variation of the heat exchanging rate, the temperature contours at the external wall of the tubes are shown at the *right*. The *green lines* are *tube* 1; the *red lines* are *tube* 2 and the *blue lines* are *tube* 3 respectively.

Figure 11 Maximum temperature difference of reactor tubes in radial direction. The *black line* is the result with contour flow and the *red line* is the result with parallel flow.

correspond to the stagnation zones marked in Fig. 9. In addition, the maximum temperatures are commonly observed at the downstream of the tubes opposite to the flow, where is protected by the tubes, i.e. the side close to the shell in the plate-ring sections and the side far from the shell in the ring-plate sections.

4.5 Field Synergy Analysis of Heat Transfer

For the traditional design of the heat exchanger, the flow directions at the tube side and at the shell side are opposite, in order to increase the average temperature difference at two sides. However, a shell-and-tube reactor prefers to keep the temperature at tube side within a proper range in order to maintain the activity of the catalyst and the reacting rate. A optimal organization of the molten salt flow can improve the uniformity of the temperature at tube side thus the reactor performance. As discussed previously, in the present case, the heat exchanging rate in the plate-ring sections is high but the temperature of the molten salt is low, while that is opposite in the ring-plate sections. The uniformity of the heat exchanging rate is poor. In addition, the chemical heat released in the upper region in Part II is more than that in the lower region (see Fig. 8). The colder molten salt may be used to cool down the hotter reacting gases by changing the flow direction at shell side.

Two cases with counter flow and parallel flow at shell side are performed in order to understand the effects of the flow direction on the reactor performance. The maximum
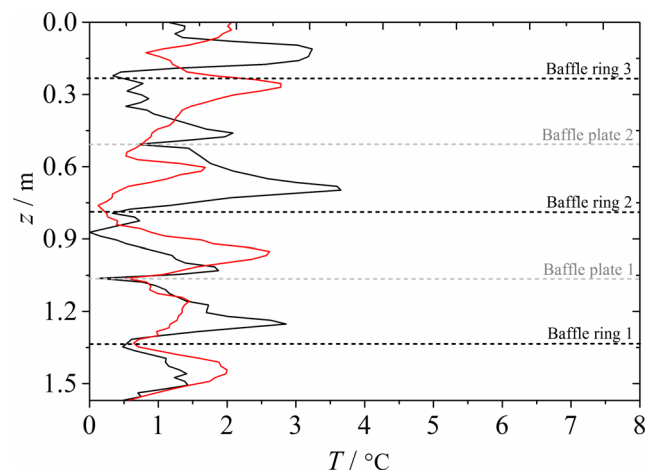
temperature difference in the three reactor tubes (see *tube* 1, *tube* 2 and *tube* 3 in Fig. 10) in axial direction is reduced from 6.3 °C, 5.2 °C and 4.3 °C with counter flow to 4.7 °C, 3.8 °C and 3.0 °C with parallel flow. Hence, the parallel flow may improve the uniformity of the temperature of the reaction tubes in axial direction. Meanwhile, the parallel flow can reduce the maximum temperature in the sections II and IV and increase that in the sections I III and V. Figure 11 shows the effects of the molten salt flow direction on the maximum temperature difference of the reaction tubes at the same cross section in Part II. In the case of counter flow, the maximum difference is 3.7 °C, which is 2.9 °C in the case of parallel flow. Similar results are obtained in Parts I and III. Therefore, it is concluded that the parallel flow demonstrates better performance by reducing the temperature difference in the reactor and improving the temperature uniformity in the reaction tubes.

5 Conclusions

The present paper purposed a Zonal Different-Time-Step algorithm which could be applied for simulating the flow, chemical reaction and heat transfer couple closed system. This method decomposed the domain into the reaction zone and the flow zone and the CFD simulations were individually performed in each zone. They swapped the data at the interface between them via interpolation. The ZDTS significantly improved the computational efficiency by reducing the data exchanging frequency between the zones and saving the computational cost in the reaction zone.

The ZDTS was successfully applied for understanding the heat transfer of a shell-and-tube reactor. The results indicated that the high order interpolation method could capture the rapid variation of the variables, which might yield better results in the zones with complicated flow. In addition, the ZDTS could provide the comprehensive physical information, i.e. the flow field and the temperature distribution, offer the accurate prediction on the positions of the stagnation zones and the dead zones and reveal the characteristic of the heat transfer between the shell side and the tube side.

Af was a critical parameter in the ZDTS, representing the coupling frequency between the flow zone and the reactor zone, which value might be obtained empirically. A smaller Af implied that the data may be swapped more frequently between each zone, hereby higher computational amount was expected, and vice versa. A series simulation showed that $Af = 5 \sim 10$ was recommended for the present study. The numerical results showed good agreement with the experimental results while the computational cost decreased about 50 %.

References

1. Aglulin, A. (2014). Kinetics and possible mechanism of hydrogen chloride oxidation over supported copper-containing salt catalysts: I. Kinetics of hcl oxidation in the deacon and methane oxychlorination reactions over a copper-potassium salt catalyst. *Kinetics and Catalysis*, *55*(5), 571–581.

2. Arkilic, E.B., Schmidt, M., Breuer, K.S., et al. (1997). Gaseous slip flow in long microchannels. *Journal of Microelectromechanical Systems*, *6*(2), 167–178.

3. Bao, Z., Wu, Z., Nyamsi, S.N., Yang, F., & Zhang, Z. (2013). Three-dimensional modeling and sensitivity analysis of multi-tubular metal hydride reactors. *Applied Thermal Engineering*, *52*(1), 97–108.

4. Baptista, C.G., & Castro, J.A. (1993). Cell models for the shell-side flow in multitubular reactors. *Industrial & Engineering Chemistry Research*, *32*(6), 1093–1101.

5. Benkenida, A., Bohbot, J., Jouhaud, J.C., Benkenida, A., Jonville, G., Darracq, D., Bohbot, J., Garnier, J., Toumit, S., Darracq, D., & et al. (2001). Patched grid and adaptive mesh refinement strategies for wake vortex transport calculation. In *Proceeding of the AIAA applied aerodynamics conference*. Anaheim: AIAA.

6. Bird, R.B., & Stewart, W.E. (1960). *Lightfoot transport phenomena*. New York: Wiley.

7. De Morais, E.R., Lunelli, B.H., Jaimes, R.R., De Souza Victorino, I.R., Maciel, M.R.W., & Filho, R. (2011). Development of an industrial multitubular fixed bed catalytic reactor as cape-open unit operation model applied to ethene production by ethanol

8. Franklin, J.D., & Lee, J.S. (2010). A high quality interpolation method for colocated polyhedral/polygonal control volume methods. *Computers & Fluids*, *39*(6), 1012–1021.

9. Hsu, C., & Cheng, P. (1990). Thermal dispersion in a porous medium. *International Journal of Heat and Mass Transfer*, *33*(8), 1587–1597.

10. Liang, Q., Guo, X., Dai, Z., Liu, H., & Gong, X. (2012). An investigation on the heat transfer behavior and slag deposition of membrane wall in pilot-scale entrained-flow gasifier. *Fuel*, *102*, 491–498.

11. Novosselov, I., Malte, P., Yuan, S., Srinivasan, R., & Lee, J. (2006). Chemical reactor network application to emissions prediction for industial dle gas turbine. In *ASME turbo expo 2006: Power for land, sea, and air* (pp. 221–235). American Society of Mechanical Engineers.

12. Ozden, E., & Tari, I. (2010). Shell side cfd analysis of a small shell-and-tube heat exchanger. *Energy Conversion and Management*, *51*(5), 1004–1014.

13. Ruthven, D.M. (1984). *Principles of adsorption and adsorption processes*. Wiley.

14. Stankiewicz, A. (1989). Advances in modelling and design of multitubular fixed-bed reactors. *Chemical Engineering & Technology*, *12*(1), 113–130.

15. Stankiewicz, A., & Eigenberger, G.G. (1991). Dynamic modelling of multitubular catalytic reactors. *Chemical Engineering & Technology*, *14*(6), 414–420.

16. Yang, Y., Zhu, C., Gu, Z., Shang, L., & Dick, R.P. (2006). Adaptive multi-domain thermal modeling and analysis for integrated circuit synthesis and design. In *IEEE/ACM International Conference on Computer-aided design, 2006. ICCAD'06*. IEEE.

17. Zhan, Y., & Sapatnekar, S.S. (2005). *A high efficiency full-chip thermal simulation algorithm*, (pp. 635–638). IEEE Computer Society.

18. Zhang, S., Chen, F., & Liu, H. (2014). Multi-field coupling numerical analysis approach for aerothermal environment of hypersonic vehicles. *Acta Aerodynamica Sinica*, *2*, 861–867.

19. Zhao, X., Sun, Z., Tang, L., & Zheng, G. (2011). Coupled flow-thermal-structural analysis of hypersonic aerodynamically heated cylindrical leading edge. *Engineering Applications of Computational Fluid Mechanics*, *5*(2), 170–179.

dehydration process. *Chemical Engineering Transactions*, *24*, 403–408.

Dr. Ke Wu received his B.S. degree in water resource engineering from Zhejiang University in 2002, and the Ph.D. degree in civil engineering from Zhejiang University in 2008. He is currently a assistant researcher in College of Civil Engineering and Architecture, Zhejiang University, and also a visiting scholar at Taiwan Ocean University from 2015 to 2016. His academic specialties are computational fluid dynamic simulation on the issue of fluid flow, heat and mass transfer. He has published over 40 academic papers in journals.
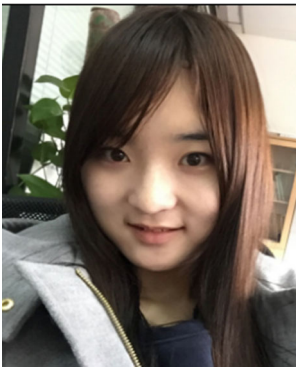
Dr. Kai Zhu received his B.S. degree in School of Energy and Environment, Southeast University, China, in 2010, and Ph.D. degree in College of Civil Engineering and Architecture, Zhejiang University, China, in 2015. He is currently a Lecture in College of Quality and Safety Engineering, China Jiliang University. His current research interests include novel flame retardant materials, modeling in flow and heat transfer, and safety in underground space. He has published more than 20 academic papers in these areas.

Cheng Kang received his B.S. degree in Xuhai College, China University of Mining & Technology, Xuzhou, China, in 2010, his M.S. degree in School of Civil Engineering and Architecture, Anhui University of Science & Technology, Huainan, China, in 2014. He is currently Ph.D. candidate in College of Civil Engineering and Architecture, Zhejiang University, Hangzhou, China. His research interests cover tunnel lighting and environment.

Xin Zhang received her B.S. degree in School of Electronic Engineering from Xi'an Shiyou University, Xi'an, China, in 2012. She is currently pursuing the Ph.D. degree in College of Civil Engineering and Architecture, Zhejiang University, Hangzhou, China. Her research focuses upon tunnel ventilation control and pollutant discharge.

Dr. Yanji Wei obtained his doctor's degree from the Mathematics and Statistics, University College Dublin, Ireland. His research is on numerical modeling of wave energy converter. Prior to his PhD study, He has been working in Second Institute of Oceanography in China. Currently he focuses on CFD simulations of various engineering problems.